CrossMark

ORIGINAL PAPER

Seismic damage assessment based on regional synthetic ground motion dataset: a case study for Erzincan, Turkey

Shaghayegh Karimzadeh[1] · Aysegul Askan[2] · Murat Altug Erberik[1] · Ahmet Yakut[1]

Abstract Estimation of seismic losses is a fundamental step in risk mitigation in urban regions. Structural damage patterns depend on the regional seismic properties and the local building vulnerability. In this study, a framework for seismic damage estimation is proposed where the local building fragilities are modeled based on a set of simulated ground motions in the region of interest. For this purpose, first, ground motion records are simulated for a set of scenario events using stochastic finite-fault methodology. Then, existing building stock is classified into specific building types represented with equivalent single-degree-of-freedom models. The response statistics of these models are evaluated through nonlinear time history analysis with the simulated ground motions. Fragility curves for the classified structural types are derived and discussed. The study area is Erzincan (Turkey), which is located on a pull-apart basin underlain by soft sediments in the conjunction of three active faults as right-lateral North Anatolian Fault, left-lateral North East Anatolian Fault, and left-lateral Ovacik Fault. Erzincan city center experienced devastating earthquakes in the past including the December 27, 1939 (Ms = 8.0) and the March 13, 1992 (Mw = 6.6) events. The application of the proposed method is performed to estimate the spatial distribution of the damage after the 1992 event. The estimated results are compared against the corresponding observed damage levels yielding a reasonable match in between. After the validation exercise, a potential scenario event of Mw = 7.0 is simulated in the study region. The corresponding damage distribution indicates a significant risk within the urban area.

Keywords Erzincan · Regional seismicity · Stochastic finite-fault method · Local buildings · Fragility analysis · Nonlinear time history analysis

✉ Aysegul Askan
aaskan@metu.edu.tr

[1] Civil Engineering Department, Middle East Technical University, 06800 Ankara, Turkey

[2] Civil Engineering and Earthquake Studies Departments, Middle East Technical University, 06800 Ankara, Turkey

1 Introduction

Seismic loss estimation is crucial in seismically active urban areas, for disaster management and risk mitigation purposes. Loss assessment traditionally has two major components: the seismic hazard (computed within a probabilistic or deterministic framework) and the building vulnerability information (e.g., Kappos et al. 1998; Yong et al. 2002; Yakut et al. 2006; Hsieh et al. 2013; Tesfamariam and Goda 2015). There is a trade-off between cost and accuracy of the estimations depending on the level of data and model complexity used in hazard and vulnerability stages.

Damage patterns evaluated in the aftermath of large earthquakes indicate that the distribution of seismic damage is a function of the local seismic excitations and properties of building stock. Thus, it is important to develop feasible techniques that consider local properties within reasonable accuracy to determine potential damages in urban areas. This study concentrates on a novel approach for seismic damage assessment based on simulated ground motions and local building data. Simulations are particularly preferred herein since they provide complete sets of records compatible with the regional seismic properties. Previously, simulated motions were used as input records in seismic damage and loss estimations (e.g., Ugurhan et al. 2011; Sørensen and Lang 2014). However, seismic damage estimations for a population of buildings have not been performed using fragility models derived with simulated motions. In this study, a set of scenario earthquakes in the study area is simulated with regional seismic properties such as source, path, and local site models. These records are then used as input to nonlinear analyses of local building models that are formed with information from walk-down surveys. Next, using response statistics of these seismic analyses, fragility curves are derived. These curves reflect the local seismic demand and resistance to yield accurate damage estimations.

The proposed method is initially validated by an application in Erzincan (Turkey). The city is particularly selected due to the sparse ground motion network despite the significant seismic activity. Simulations provide alternative time series for such cases. In addition, it is an urban area including a variety of building structures with a range of seismic performance levels. After validation of the proposed framework, prediction of ground motions and damage levels are performed for a potential event in the same area.

2 Study region

North Anatolian Fault Zone (NAFZ) is an active right-lateral strike-slip fault in the northern part of Turkey (Fig. 1a). This fault runs along the transform boundary between Eurasian plate and Anatolian plate. The March 13, 1992 Erzincan earthquake with Mw = 6.6 (Fig. 1b) is one of the devastating earthquakes, originating from the eastern part of North Anatolian Fault (NAF). This earthquake caused more than 500 fatalities in Erzincan and an economic loss of 5–10 trillion Turkish Liras (Akinci et al. 2001). In addition to the 1992 event, Erzincan had suffered from another destructive earthquake in 1939 (Mw ∼ 8) that had led to significant structural damage as well as mortalities (Fig. 1b).

Erzincan is one of the most hazardous cities in Turkey with tectonically complicated area, in the conjunction of three strike-slip faults: the right-lateral North Anatolian Fault, the left-lateral North East Anatolian Fault, and the left-lateral Ovacik fault. Erzincan has developed as a pull-apart basin with moderate size (50×15 km^2) along the interactions in

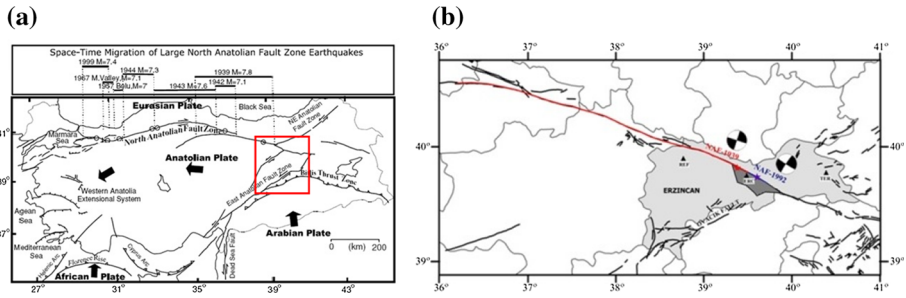**(a)**   **(b)**

Fig. 1 a Major tectonic structures around the Anatolian plate and major earthquakes on the North Anatolian Fault Zone within the last century (Akyuz et al. 2002), **b** Seismotectonics of the Erzincan region which is shown with the red rectangle in part (**a**), with the fault systems and the epicenters of the 1939 and 1992 events (Askan et al. 2013)

between Ovacik and North Anatolian Faults. Alluvial deposits have considerable thickness at the center of the basin compared to the borders near the mountains. There are two reasons for considering Erzincan region as our case study. First, the eastern part of NAFZ is relatively less investigated than western part of it. Second, there exist sparse ground motion data in the records of eastern part of NAFZ.

In this study, information related to the building inventory in the region is obtained from the database of the General Statistic Agency in Turkey (TUIK) (http://www.tuik.gov.tr/Web2013/iletisim/iletisim.html) and the site survey carried out by a technical team including the authors of this work. The obtained information reveals that the building stock in Erzincan city is composed of masonry (57) and RC (43%) structures. The city center contains a variety of buildings that perform many different functions. However, majority of the buildings in Erzincan (79%) is residential. Thus, the focus of this study is damage estimation of only the residential buildings.

3 Ground motion simulations

In regions with sparse ground motion data, ground motion simulations provide alternative regional time histories accounting for the specific features of the fault and the kinematics of the rupture process. Recently, simulated motions are being used for engineering purposes. The next section presents a brief discussion of the strong ground motion simulation methodology used herein followed with an application for generation of scenario earthquakes in Erzincan.

3.1 Methodology: stochastic ground motion simulations

All ground motion simulation techniques aim to estimate physically modeled synthetic time histories. For different methods, various levels of precision and cost can be achieved relying on modeling assumptions and solution approaches. Ground motion simulation techniques can be categorized into three major groups: deterministic, stochastic, and hybrid simulations. In deterministic approaches, which involve numerical solution of the wave equation for full wave propagation purposes, well-defined seismic sources and highly resolved velocity models are required (e.g., Frankel 1993; Olsen et al. 1996). These approaches are particularly useful for simulating lower frequency ground motions as a

result of the computational and physical constraints corresponding to the minimum wavelength regardless of their accuracy. Stochastic techniques combine the spectral amplitude of ground motion with a random phase spectrum (Boore 1983). These methods have intrinsic limitations due to the absence of full wave propagation effects; however, they are used efficiently worldwide for simulating higher frequency ground motions (e.g., Beresnev and Atkinson 1964; Motazedian and Atkinson 2005; Ugurhan and Askan 2010). Hybrid methods combine deterministic and stochastic approaches for the simulation of low- and high-frequency components, respectively. They are developed for simulation of broadband ground motion records (e.g., Kamae et al. 1998; Pitarka et al. 2000; Mai et al. 2010).

In this study, a recent form of stochastic finite-fault modeling which was shown to provide realistic broadband frequencies for engineering purposes is used. Since there exist no high-resolution velocity models of shallow soil layers for Erzincan region, deterministic and hybrid models are out of scope.

In stochastic finite-fault methodology, the rectangular fault plane is divided into subfaults with specified width and length sizes to consider the effects of finite dimension of fault plane. The contributions of all of these subfaults are summed in time domain by considering each subfault as a single point source with an w^{-2} spectrum (Hartzell 1978). It is assumed that the hypocenter is located at the center of one of subfaults and the rupture initiates propagating radially from the hypocenter by a constant rupture velocity. Each subfault is triggered when the rupture reaches the center of that subfault. Finally, to calculate the final ground motion from the entire fault at the receiver, contributions of all subfaults are summed in time domain by taking into account of the corresponding time delay of each subfault. In the dynamic corner frequency concept, the total energy radiated from the fault is conserved regardless of the selected subfault size. In this study, the dynamic corner frequency approach as implemented in the computer program EXSIM (Motazedian and Atkinson 2005) is used.

The acceleration spectrum $A_{ij}(f)$ of the ijth subfault is defined in terms of source, path, and site effects as follows:

$$A_{ij}(f) = CM_{0ij}H_{ij}\left[(2\pi f)^2 / \left[1 + \left(\frac{f}{f_{c_{ij}}}\right)^2\right]\right] e^{-\frac{\pi f R_{ij}}{Q(f)\beta}} G(R_{ij}) A(f) e^{-\pi \kappa f}, \tag{1}$$

where $C = \frac{\Re^{\theta\varphi} \cdot \sqrt{2}}{4\pi\rho\beta^3}$ is a scaling factor, $\Re^{\theta\varphi}$ is the radiation pattern, ρ is the density, β is the shear wave velocity, $M_{0ij} = \frac{M_0 S_{ij}}{\sum_{k=1}^{nl} \sum_{l=1}^{nw} S_{kl}}$ is the seismic moment, S_{ij} is the relative slip weight, and $f_{c_{ij}}(t)$ is the dynamic corner frequency of the ijth subfault, where $f_{c_{ij}}(t) = N_R(t)^{-1/3} 4.9 \times 10^6 \beta \left(\frac{\Delta\sigma}{M_{0_{ave}}}\right)^{1/3}$. Here, $\Delta\sigma$ is the stress drop, $N_R(t)$ is the cumulative number of ruptured subfaults at time t, and $M_{0_{ave}} = M_0/N$ is the average seismic moment of subfaults. R_{ij} is the distance from the observation point, $Q(f)$ is the quality factor, $G(R_{ij})$ is the geometric spreading factor, $A(f)$ is the site amplification term, and $e^{-\pi\kappa f}$ is a high-cut filter included to provide the spectral decay at high frequencies described with the Kappa factor of soils (Anderson and Hough 1984). H_{ij} is a scaling factor introduced to conserve the high-frequency spectral level of the subfaults.

3.2 Simulations along eastern segment of NAFZ

In this section, it is aimed to perform ground motion simulations for scenario earthquakes of size Mw = 5.0, 5.5, 6.0, 6.5, 7.0, and 7.5 as well as the 1992 event using stochastic finite-fault methodology (Motazedian and Atkinson 2005). All of these scenario events are generated on the same fault where the 1992 Erzincan event (Mw = 6.6) occurred (Fig. 1b). During simulations, the epicenter of all scenario earthquakes is kept similar as the epicenter of the 1992 earthquake since the epicenter of the 1992 earthquake is critical in terms of its close distance to the city center.

In the present study, the region of interest is defined as a rectangular box bounded by 39.45°–39.54° longitudes, 39.70°–39.78° latitudes. To simulate full time series of ground motions, a total of 123 grid points are selected inside of this region. Figure 2 shows distribution of these nodes in the interested area. Among 123 nodes, 90 of them represented by red circle symbols are selected with a distance of approximately 1 km from each other. Twenty-four of the nodes shown by black triangular symbols correspond to the coordinates
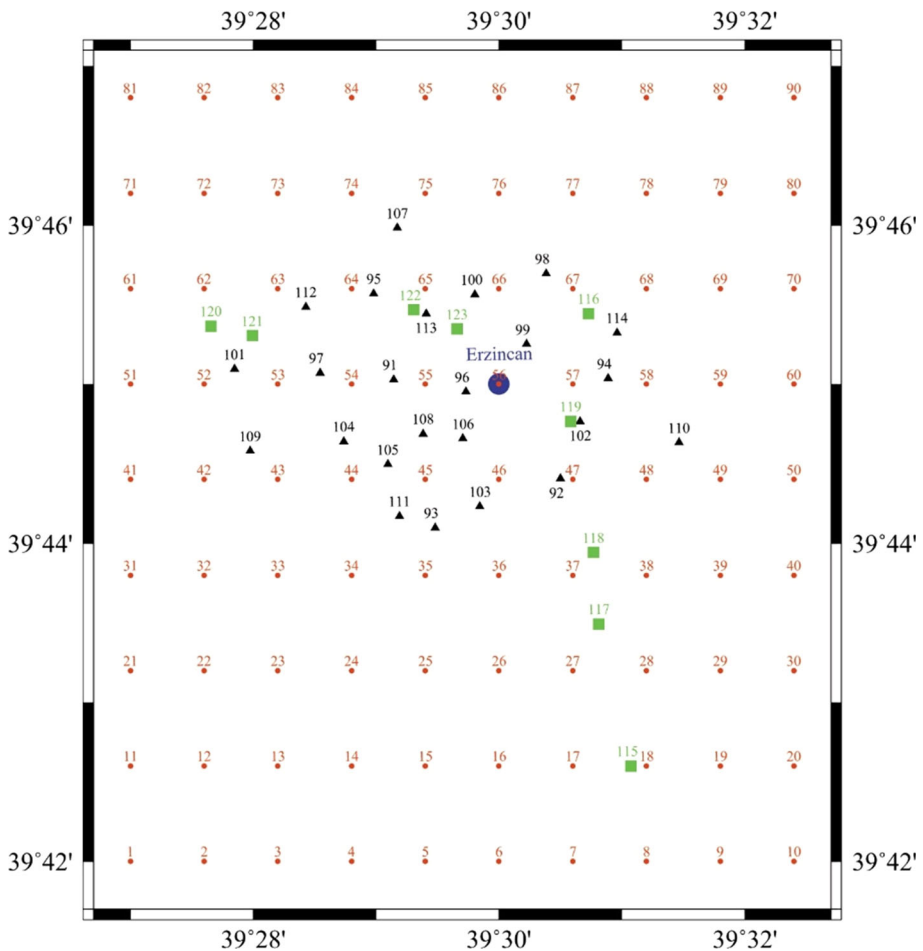

Fig. 2 Distribution of the selected nodes in the study area

of all streets in the Erzincan region. Finally, nine of these nodes represented by green rectangular symbols are the stations where there exist the shear wave velocity soil profiles for them. The existing shear wave velocity profiles at nine nodes were obtained by a microtremor array method, details of which are explained in Askan et al. (2015b). However, there is no detailed information regarding the soil conditions of the other nodes. Therefore, the Vs30 of the closest station is assigned to each grid point. Figure 3a, b presents the simulated sample acceleration time histories along with Fourier amplitude spectra, respectively, for the scenario events of Mw = 6.0 and Mw = 7.0 at the selected five nodes (1, 10, 56, 81, and 90 as given in Fig. 2) inside the Erzincan region. Table 1 presents information on the soil types in terms of Vs30 values, the Joyner and Boore (R_{JB}) distances, and PGA values corresponding to the selected five nodes for scenario events of Mw = 6.0 and Mw = 7.0. It is observed that nodes which are closer distances from the fault plane and located on softer soil conditions experience larger values of PGA and FAS amplitudes as compared to the nodes which have farther source to site distances and those on harder soil sites.

For generation of synthetic ground motions at the selected nodes, the source, path, and site parameters for the simulations are adopted from a previous study by Askan et al. (2013). In this study, the validity of these parameters was obtained by comparing the generated ground motion time histories with those observed during the 1992 Erzincan earthquake. Table 2 displays the parameters employed in the simulations.

Figures 4 and 5 illustrate the spatial distribution of the simulated peak ground acceleration (PGA) and peak ground velocity (PGV) within the city center for the 1992 Erzincan earthquake (Mw = 6.6) as well as the scenario event with Mw = 7.0 as two samples, respectively. Each synthetic record is baseline corrected and fourth-order band-pass filtered at 0.25–25 Hz. The results of the 1992 Erzincan earthquake simulation yield that the city center experiences maximum PGA and PGV values of around 1 g and 85 cm/s, respectively. As stated previously, Erzincan city center is placed on a deep alluvial basin in the close vicinity of the fault plane. It was recorded that, in spite of the moderate size of 1992 Erzincan earthquake, the residential structures suffered from significant levels of damage during the earthquake. Thus, these higher amplitudes of anticipated ground motions are believed to explain the observed widespread damage. When the results of the scenario event with Mw = 7.0 are studied, it is observed that the maximum values of PGA and PGV are anticipated as 1.44 g and 110 cm/s, respectively.

4 Identification and idealization of the regional building stock

This section deals with the identification and idealization of the building stock in the study region, i.e., the Erzincan city. First, the classification and the distribution of the building stock are determined based on the available building census data from TUIK (http://www.tuik.gov.tr/Web2013/iletisim/iletisim.html) and the observed data during the field survey as mentioned in Sect. 2. Next, the structural characteristics of the existing construction types in the region are idealized by using equivalent single-degree-of-freedom (ESDOF) models. A well-known hysteresis model is used in order to obtain the response statistics of the ESDOF models through nonlinear time history analyses (NLTHA). In the next section, this information is used to derive the fragility curve sets of the ESDOF models corresponding to different building subclasses.
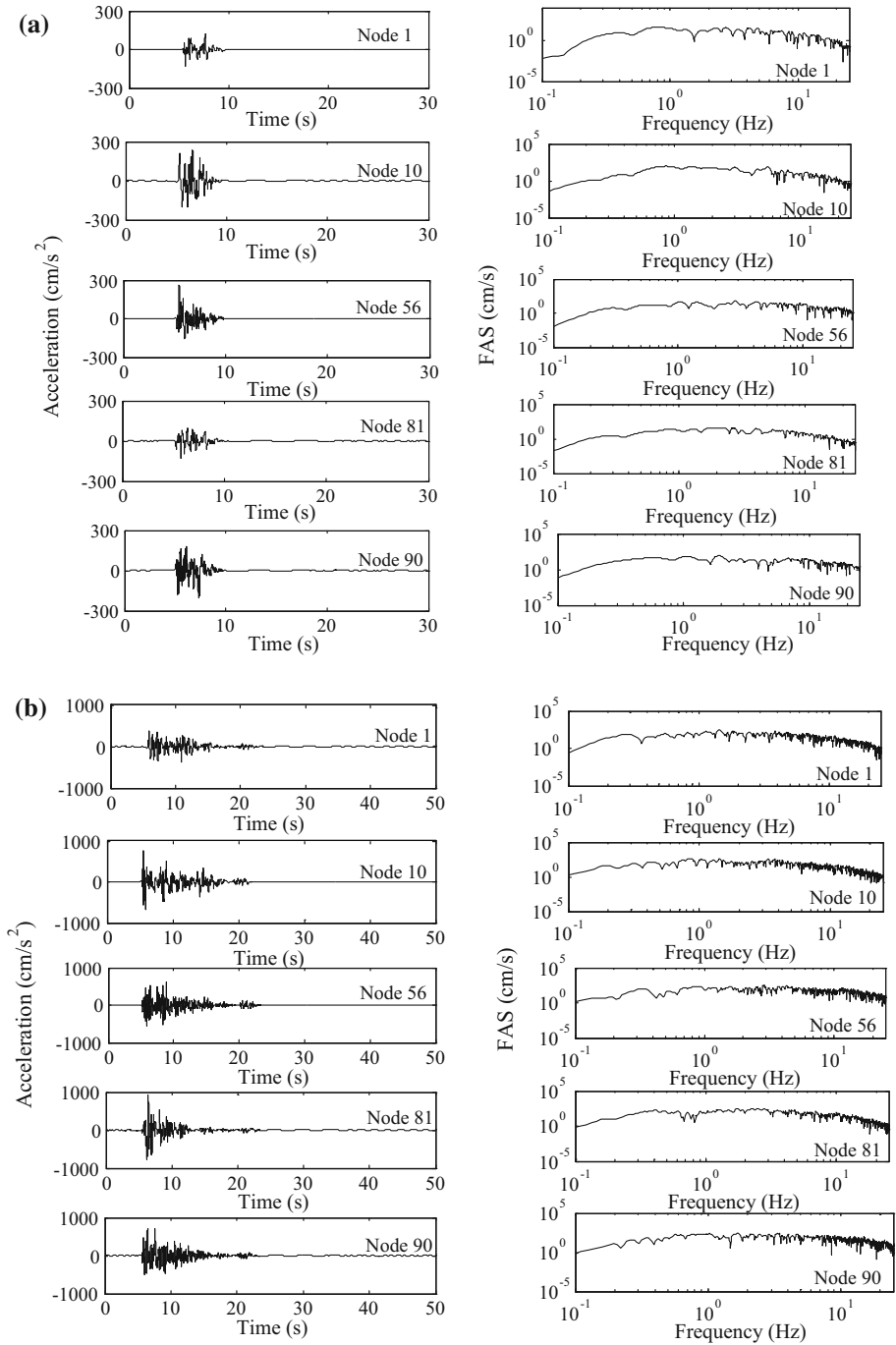
Fig. 3 Simulated acceleration time histories and Fourier amplitude spectra at the selected five nodes inside of the Erzincan region for the scenario event of **a** Mw = 6.0, **b** Mw = 7.0

Table 1 Information on Vs30 values, R_{JB} distances, PGA values at the selected 5 stations for scenario events of Mw = 6.0 and Mw = 7.0

Node ID	Vs30 (m/s) (Askan et al. 2015b)	Mw = 6.0		Mw = 7.0	
		R_{JB} (km)	PGA (cm/s²)	R_{JB} (km)	PGA (cm/s²)
1	368	14.18	130.04	8.00	372.05
10	262	7.90	231.82	3.58	771.92
56	474	8.58	264.63	1.00	601.00
81	368	13.18	128.93	0.73	935.26
90	483	5.90	205.45	3.69	714.00

Table 2 Simulation parameters used in the simulation of scenario earthquakes

Parameter	Value
Hypocenter location	39°42.3N, 39°35.2E
Hypocenter depth	9 km
Depth to the top of the fault plane	2 km
Fault orientation	Strike: 125°, dip: 90°
Fault dimensions	Wells and Coppersmith (1994)
Crustal shear wave velocity	3700 m/s
Rupture velocity	3000 m/s (Askan et al. 2013)
Crustal density	2800 kg/m³
Stress drop	Mohammadioun and Serva (2001)
Quality factor	$Q = 122f^{0.68}$
Geometrical spreading	$R^{-1.1}, \quad R \leqslant 25\,\text{km}$
	$R^{-0.5}, \quad R > 25\,\text{km}$
Duration model	$T = T_0 + 0.05R$
Windowing function	Saragoni–Hart
Kappa factor	Regional kappa model [$k_0 = 0.066$, Askan et al. (2013)]
Site amplification factors	Local soil model (Askan et al. 2015b)

4.1 Identification of the building stock

The building census data obtained from TUIK provide general information regarding the building inventory in the region in terms of the major construction types. However, this is not up-to-date information and it is too broad in order to classify the buildings according to their local characteristics and to estimate the regional seismic damage distribution. Hence, a site survey was conducted in the Erzincan city by a technical team including the authors of this study in order to update the available building data and to identify the local construction types with their specific characteristics. Based on the results of this site survey in the city center of Erzincan, the residential building stock is classified into 21 groups including 12 RC and nine masonry subclasses. Among these subclasses, RC buildings are considered as either frame type, shear wall type (referred to as tunnel form), or dual type
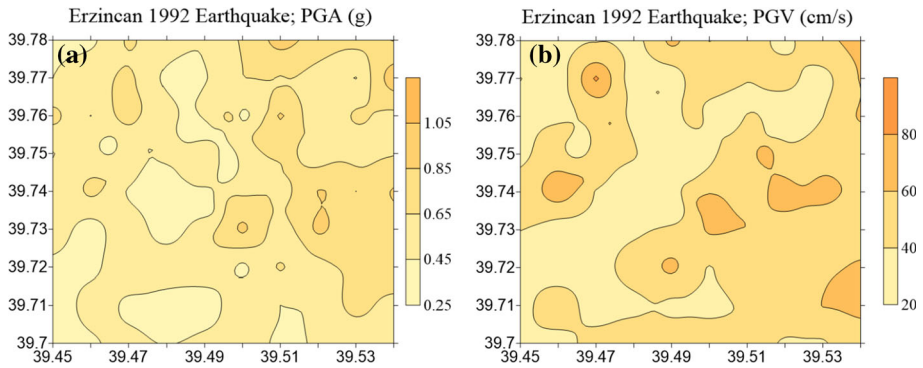
Fig. 4 Spatial distribution of the simulated, **a** PGA, **b** PGV values of the 1992 Erzincan earthquake
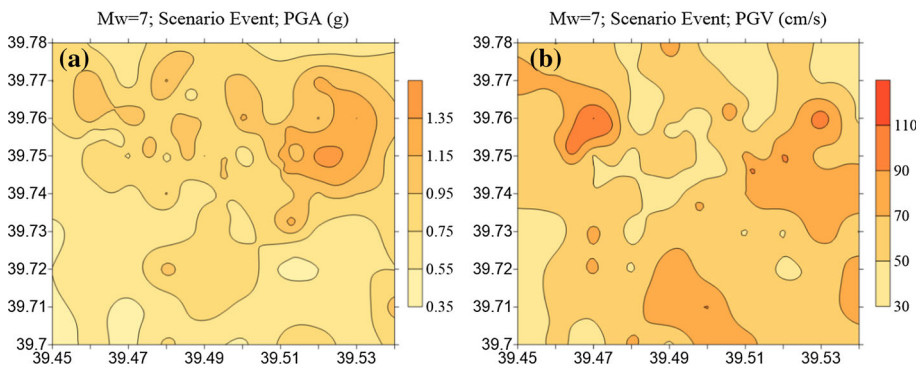

Fig. 5 Spatial distribution of the simulated, **a** PGA, **b** PGV values of the scenario earthquake with Mw = 7.0 in Erzincan region

(i.e., frame with shear walls). Structural parameters used in the classification of buildings are structural type, number of stories, and level of compliance with the seismic design and construction principles. In classification of all subclasses, the first two letters in the abbreviated names account for the type of structural system, where 'RF' stands for RC frame buildings, 'RW' for RC tunnel form, 'RH' for RC dual type, and 'MU' for masonry subclasses. The number in the next digit indicates the number of stories, where for masonry, classes '1,' '2,' or '3' represent one-story, two-story, or three-story, and for all three RC groups, '1' or '2' indicate whether the building is low rise (number of stories is between 1 and 3) or mid rise (number of stories is between 4 and 8), respectively. The letter in the last digit 'A,' 'B,' or 'C' denotes the high, moderate, and low level of compliance with seismic design codes and construction principles, respectively. For example, RF2A represents earthquake-resistant mid-rise RC frame buildings, whereas MU2C represents deficient two-story masonry buildings.

4.2 Idealization based on ESDOF models

In regional damage estimation, it is generally preferred to use simplified and idealized structural models to simulate the seismic response statistics of large building populations

for the sake of computational efficiency. Accordingly, in this study, each building subclass is represented through an idealized ESDOF model by specifying three basic structural parameters; period (T), strength ratio (η), and ductility factor (μ). This simplified approach has been employed in earthquake engineering for a long time that goes back to the early work of Biggs (1964), followed by many markable studies (Saiidi and Sozen 1981; Fajfar and Fischinger 1988; Qi and Moehle 1991). The ESDOF approach was also employed in the well-known guidance documents, i.e., (ATC-40 1996; BSSC 1997). There are two gross assumptions while using ESDOF systems. First, the global response of a multi-degree-of-freedom system is assumed to be represented by a single deformed shape, which is eventually the fundamental mode shape. Second, this deformed shape is assumed to remain constant during the response. In this study, it is considered that the use of ESDOF models and, in turn, these two assumptions are justifiable since the study deals with a population of ordinary residential buildings instead of individual and specific buildings, in which there should be a trade-off between precision and computational effort. Furthermore, the field observations revealed that the surveyed residential buildings are generally regular in plan and elevation with nearly homogeneous distribution of floor mass and stiffness leading to first-mode dominant response, which are in favor of the above assumptions for ESDOF systems.

Since NLTHA are conducted to obtain the response statistics of ESDOF models, a robust hysteresis model is required to simulate the inherent cyclic characteristics of each building subclass under earthquake excitations. As a matter of fact, new and well-constructed structures are expected to exhibit almost none or slight degradation. However, most existing buildings in Turkey include many structural deficiencies, which result in rapid degradation of stiffness and strength along with decreased energy dissipation capacity. Therefore, the most accurate hysteresis models are the ones which include strength and stiffness deterioration features that are critical for demand predictions during major earthquakes. Few of the hysteresis models integrate various modes of cyclic deterioration in strength and stiffness such as basic strength, post-capping strength, uploading stiffness, and reloading stiffness deterioration that may be observed in the real inelastic behavior. In this study, to assess the effect of deterioration characteristics of structural systems on the final fragility curves, among different hysteresis models, the one proposed by Ibarra et al. (2005), named as 'Modified Ibarra–Medina–Krawinkler Deterioration Model,' is applied. Ibarra et al. (2005) verified that their hysteresis peak-oriented deterioration model is able to predict the inelastic dynamic response of reinforced concrete structures during collapse with an acceptable degree of accuracy. The proposed deterioration model has then been used in different studies and for different structural types (Ibarra and Krawinkler 2005; Lignos and Krawinkler 2010, 2012), and the results of these studies seem to be promising.

Figure 6 illustrates the backbone curve of the modified Ibarra–Medina–Krawinkler deterioration model with peak-oriented hysteretic response. The model is based on the fundamental hysteretic rules suggested by Clough and Johnston (1966). However, the modified Ibarra–Medina–Krawinkler deterioration model contains strength capping as well as residual strength compared to the one proposed by Clough and Johnston. In the backbone curve, parameters K_e, F_y, and α_s correspond to the elastic (initial) stiffness, the yield strength, and the strain hardening ratio ($\alpha_s = K_s/K_e$), respectively. Here, K_s describes the pre-capping stiffness. In this model, deterioration of the backbone curve is initiated by a softening branch with a cap deformation of δ_c that corresponds to the deformation of the peak strength of the force–deformation curve. The ratio of the cap deformation (δ_c) to the yield deformation (δ_y) is denoted as the ductility capacity, ($\mu = \delta_c/\delta_y$). The parameter α_c is
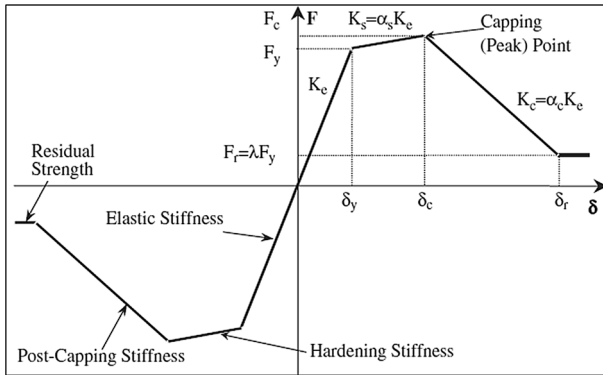
Fig. 6 Backbone curve for hysteresis model (adopted from Ibarra et al. (2005))

the ratio of the post-capping stiffness to the elastic stiffness, which has generally a negative value, $(\alpha_c = K_c/K_e)$. Residual strength is represented by F_r, which is considered as a fraction of the yield strength, $(F_r = \lambda F_y)$. Besides, the deformation corresponding to the residual strength is abbreviated as δ_r.

In addition to a post-capping negative stiffness branch of the backbone curve to capture in-cyclic deterioration, the modified Ibarra–Medina–Krawinkler peak-oriented hysteretic model includes cyclic modes of strength and stiffness deterioration based on the cumulative hysteresis energy dissipation. Four individual cyclic deterioration modes are basic strength, post-capping strength, unloading stiffness, and reloading stiffness deterioration that may be activated beyond the elastic limit at least in one direction. Defining the hysteretic energy dissipation parameter γ, it is possible to simulate different levels of cyclic degradation for the ESDOF models. Details about the cyclic deterioration modes can be found in Ibarra et al. (2005).

In this study, the three major structural parameters (T, η, and μ) are considered as random variables with mean and standard deviation values, whereas the other hysteretic model parameters (α_s, α_c, λ, and γ) are taken as constant with a single value. All values of the considered ESDOF parameters for each subclass are listed in Table 3. These parameter values have been obtained from various sources: literature (for Turkish residential buildings), analytical computations (from idealized capacity curves of MDOF models), and also expert judgment. The details of obtaining these ESDOF parameters are provided in Askan et al. (2015a) and Karimzadeh et al. (2015).

For all subclasses, it is observed that the period of any subclass is dependent on the type of structural system and number of stories. However, period is independent of the level of compliance of a structure with seismic design codes. Therefore, for subclasses with similar number of stories and structural types but with different levels of compliance with seismic design codes (e.g., RF1A, RF1B, RF1C), period is considered to be constant. In contrast, strength ratio and ductility factor are two parameters on which structural type, number of stories, and the level of compliance of a structure with seismic design codes all have large impact.

Table 3 Proposed SDOF parameters for all building subclasses

Frame ID	T (s)		η		μ		α_s (%)	α_c (%)	λ	γ
	Mean	SD	Mean	SD	Mean	SD				
RF1A	0.38	0.18	0.40	0.08	9.00	3.12	4	− 20	0.20	800
RF1B			0.30	0.11	7.30	2.02	4	− 25	0.20	400
RF1C			0.23	0.06	4.90	1.47	4	− 30	0.20	200
RF2A	0.70	0.27	0.34	0.11	7.10	2.25	4	− 20	0.20	800
RF2B			0.26	0.09	6.10	1.75	4	− 25	0.20	400
RF2C			0.17	0.06	5.10	1.38	4	− 30	0.20	200
RW1A	0.05	0.02	1.95	0.55	3.00	1.10	8	− 20	0.20	1200
RW2A	0.15	0.05	1.30	0.36	2.70	0.90	8	− 20	0.20	1200
RH1A	0.08	0.04	0.93	0.31	5.40	1.70	4	− 20	0.20	1000
RH1B			0.77	0.25	4.50	1.40	4	− 25	0.20	500
RH2A	0.43	0.18	0.59	0.17	4.90	1.40	4	− 20	0.20	1000
RH2B			0.47	0.13	4.00	1.20	4	− 25	0.20	500
MU1A	0.06	0.02	0.86	0.17	3.53	0.71	0	− 20	0.20	600
MU1B			0.64	0.13	3.43	0.69	0	− 25	0.20	300
MU1C			0.38	0.08	3.32	0.66	0	− 30	0.20	150
MU2A	0.12	0.03	0.69	0.17	2.75	0.69	0	− 20	0.20	600
MU2B			0.43	0.11	2.62	0.66	0	− 25	0.20	300
MU2C			0.23	0.06	2.56	0.64	0	− 30	0.20	150
MU3A	0.17	0.05	0.43	0.13	2.20	0.66	0	− 20	0.20	600
MU3B			0.27	0.08	2.12	0.64	0	− 25	0.20	300
MU3C			0.14	0.04	2.05	0.62	0	− 30	0.20	150

5 Fragility curve generation methodology

Fragility curve for a certain class of structural system is a continuous function describing the probability of exceeding a predefined damage level for specific levels of ground motion intensity. In this study, to derive the fragility curve sets of each building subclass, ESDOF models with the parameter values given in Table 3 are used in NLTHA by using a selected set of synthetic ground motion records. To perform fragility analysis, the approach can be summarized as the following four steps:

- The first step is to conduct NLTHA for the ESDOF systems defined in the previous section by using a selected set of synthetic ground motion records. In this study, OpenSees platform is used for NLTHA (http://opensees.berkeley.edu). During the analysis, variability in capacity (in terms of random variables T, $η$, and $μ$) and demand (record-to-record variability) are considered.
- In the second step, response statistics of the ESDOF models are generated due to the results of NLTHA. ESDOF displacement is selected to be the seismic demand parameter for the considered building types. Then, for each building subclass and seismic intensity level, the overall responses of ESDOF systems are collected.

- In the third step, limit states are defined for each subclass in terms of maximum displacement. In this study, three performance levels are considered as immediate occupancy (LS_1), life safety (LS_2), and collapse prevention (LS_3).
- In the final step, fragility curves are generated by using the response statistics and the limit states. The responses of all structures are compared with the predefined limit state values at each hazard intensity level. Then, the probability of the attainment or exceedance of a predefined limit state at each ground motion intensity level is calculated. Results of conditional probability with respect to the intensity level of ground motion records are plotted. The obtained curve is the fragility curve of a certain subclass derived for a specified performance level. This process is repeated for all limit states and building subclasses to obtain the complete set.

Details of the fragility curve generation methodology are given in the following sections.

5.1 Ground motion variability

Characteristics of the ground motion set have large impact on derivation of the fragility curves. Especially, in regions of high seismicity, regional characteristics of input ground motions can affect the generated fragility curves significantly. Therefore, in this study, fragility curves are developed based on regional ground motion database. Since there exist sparse ground motion networks in the study region, to consider the regional effects, the input ground motions are taken from the synthetic ground motion dataset generated by the stochastic finite-fault methodology as explained in Sect. 3.

The previous studies have revealed that PGV and PGA correlate well with inelastic response of flexible structures (RC frame) and stiffer structures (masonry), respectively (Erberik 2008a, b). Since the governing structural types in Erzincan include both RC and masonry buildings, to provide a strong correlation between hazard parameters and non-linear responses of the existing building subclasses, ground motions records selected for fragility curve generation are separated into two groups: The first group is constituted according to PGV (for RC buildings) and the second group is formed with respect to PGA (for masonry buildings) as the intensity parameter. Overall, the selected synthetic records cover a broad range of magnitudes between 5 and 7.5. The closest distance to the fault plane varies between 0.26 and 17.55 km. In order to have an even distribution for responses of the structures, each ground motion set, which is categorized according to PGV or PGA, is subdivided into 20 intensity levels by considering intervals of PGV = 5 cm/s or PGA = 0.05 g, respectively.

To account for the variability in demand, for each ground motion set, a total of 200 records are selected such that for each intensity level, there are ten time histories with different soil conditions, distance, and magnitude values.

5.2 Structural simulations and response statistics

In this study, T, η, and μ parameters are considered as random variables. Due to deficiency of theoretical evidence, determination of the most suitable probability distribution function for these random variables is not easy. However, it is observed that normal and lognormal distributions have been intensively used for this purpose in previous research. In this study, for the reasons of being a simple and physically meaningful (i.e., only positive values for the samples) function, lognormal distribution is considered for the selected random

variables. For sampling, latin hypercube sampling (LHS) method, which can be regarded as a constrained Monte Carlo method, is selected. By using the LHS method, 20 samples are generated for each of the random variables corresponding to the mean values of T, η, and μ. The remaining model parameters including α_s, α_c, λ, and γ are assumed to be constant for all 20 simulated buildings from each subclass.

For a single subclass, since there exist 20 model simulations, and the number of records in a specified intensity level (either PGV or PGA) is 10, the number of response data points for an intensity level counts as 200. Since there are totally 20 intensity groups, the number of required NLTHA on ESDOF models to obtain the response statistics becomes 4000.

5.3 Attainment of limit states

Attainment of limit states, which are defined as the performance levels of structures at some predefined thresholds, is a significant part of fragility analysis. Previous studies demonstrate that limit states affect the resulting fragility curves considerably (Erberik 2008b). Therefore, they should be established with special care.

As it is mentioned previously, three limit states considered in this study are immediate occupancy, life safety, and collapse prevention. Immediate occupancy limit state or shortly LS_1 represents the threshold between none-to-slight damage. This limit state is generally related to the stiffness of the structure. Life safety limit state or LS_2 is the performance level between light and moderate damage. Strength and deformation of the structure determine this limit state. Finally, collapse prevention limit state or LS_3 is the threshold for moderate up to collapse of the structure. In this state, major degradation in the stiffness and strength of the lateral-force resisting system as well as large permanent lateral deformation occurs. Deformation is the most common parameter that determines this limit state.

In this study, instead of complicated approaches based on detailed behavior of members, which are more suitable for individual or specific buildings, constant (deterministic) values are assigned to the limit states defined above since this study is focused on a building population composed of numerous subclasses. While determining the limit state values of building subclasses, previous studies concerning the fragility of Turkish buildings are taken into consideration (Erberik 2008a, b; Akkar et al. 2005; Kircil and Polat 2006; Ucar and Duzgun 2013). The values corresponding to the predefined limit states in terms of displacement for all subclasses are listed in Table 4. To generate fragility curves, these values are employed.

5.4 Generation of curves

Figure 7 shows the schematic representation of the applied procedure for generation of fragility curves. In Fig. 7a, distribution of a sample response statistics is plotted. In this figure, the horizontal axis shows the ground motion intensity and the vertical axis presents the response parameter. The horizontal line labeled as LS_i represents the target limit state. To show a sample probability calculation, in Fig. 7b, the scattered data of the jth ground motion intensity level (GMI_j) are selected. The conditional probability of attainment or exceedance of the ith limit state (LS_i) at the jth ground motion intensity level is calculated by using the following formula:

$$P\big[D \geqslant LS_i | GMI_j\big] = \frac{n_A}{n_T}, \tag{2}$$

Table 4 Limit states in terms of displacement for all subclasses

Frame ID	LS_1 (cm)	LS_2 (cm)	LS_3 (cm)
RF1A	1.55	6.70	12.40
RF1B	1.40	6.30	11.60
RF1C	1.32	5.80	10.70
RF2A	2.40	8.55	16.10
RF2B	2.00	8.10	15.20
RF2C	1.65	7.11	14.30
RW1A	0.40	1.00	3.30
RW2A	0.80	1.90	4.50
RH1A	0.40	1.80	5.50
RH1B	0.28	1.40	3.10
RH2A	1.60	5.90	9.50
RH2B	1.20	4.80	8.80
MU1A	0.07	0.25	1.54
MU1B	0.05	0.18	1.13
MU1C	0.03	0.10	0.87
MU2A	0.23	0.63	2.08
MU2B	0.14	0.37	1.67
MU2C	0.08	0.29	1.45
MU3A	0.32	0.954	3.125
MU3B	0.20	0.63	2.50
MU3C	0.11	0.52	1.88

where n_A is the sum of responses equal or above the ith limit state and n_T stands for the total number of responses at the jth ground motion intensity level. After repeating these processes for different intensity levels shown in Fig. 7a, the discrete fragility information presented in Fig. 7c can be obtained for a certain limit state. A cumulative lognormal distribution function is fitted to the obtained data with least squares technique as illustrated in Fig. 7d. To derive fragility curves for all building types, this process is repeated for three limit states and all 21 subclasses.

Figures 8, 9, and 10 show the final smooth fragility curves of all building subclasses. Comparison of the results shows that for a given seismic intensity level, as the number of stories increases, the potential of damage also increases for all building types. In addition, for all cases, as the level of compliance with seismic design and construction codes gets poorer, the probability of exceeding LS_3 (or in other words, experiencing collapse) increases. This trend verifies that the failure of the buildings which do not obey the earthquake-resistant design principles will be much more brittle than the ones which satisfy these principles. For LS_1, regardless of the level of compliance of structures with seismic design codes, the results of subclasses with the same number of stories and structural system are close to each other. This trend is also physically meaningful in the sense that LS_1 depends mainly on the stiffness of the structure. However, for LS_2 and especially for LS_3, the results deviate from each other, since these limit states are significantly affected by strength and displacement of the structure.

If the curves are compared with respect to the building types considered, it is observed that among RC buildings, RW subclasses have the best seismic performance followed by RH subclasses (Fig. 9). This is not surprising since these shear wall (or specifically tunnel
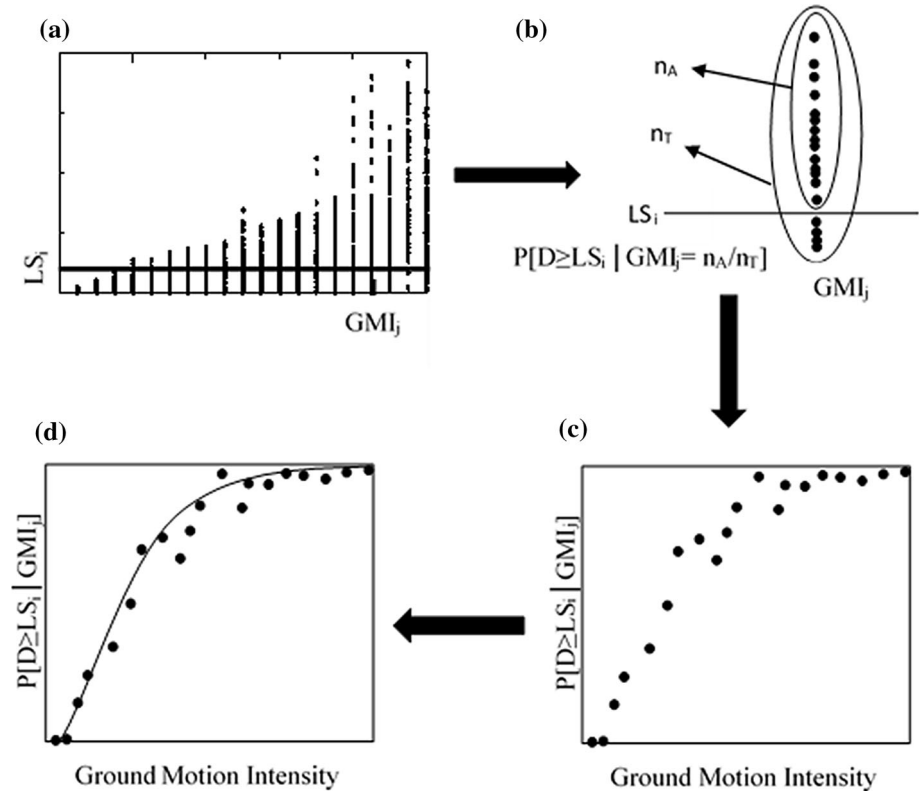
Fig. 7 Schematic representation of the fragility curve generation procedure (GMI_j represents the jth ground motion intensity level, LS_i corresponds to the ith limit state, n_A is the sum of responses equal or above the LS_i, n_T stands for the total number of responses at GMI_j, $P\left[D \geqslant LS_i|GMI_j\right]$ is the conditional probability of attainment or exceedance of LS_i at GMI_j)

form) buildings (i.e. RW subclasses) have been built in Erzincan city after the 1992 earthquake for the survivors as permanent housing (Fig. 11a). They have been designed and constructed to exhibit superior seismic performance, and until now, they have achieved this task during the previous major earthquakes in Turkey. They have a very high strength capacity; however, they do not show a very ductile global behavior due to the presence of rigid shear walls and the connections in between. This is reflected in the fragility curves such that all limit states are very close to each other, especially for RW1A. This demonstrates the narrow margin of inelastic behavior for this building type.

The RC frame buildings seem to exhibit different levels of performance depending on the specific characteristics of each subclass. As the two limiting cases, low-rise RC frame buildings that conform to the modern earthquake-resistant design principles (i.e., RF1A subclass) seem to perform well, whereas high-rise RC frame buildings that have structural deficiencies regarding seismic design principles (i.e., RF2C) exhibit poor performance under the same levels of seismic action (Fig. 8). All the other RF subclasses have seismic performance levels in between these two limiting cases as observed from the fragility curves. These trends are on justifiable grounds when compared to the field observations after major earthquakes in Turkey in the sense that the seismic performances of RC frame
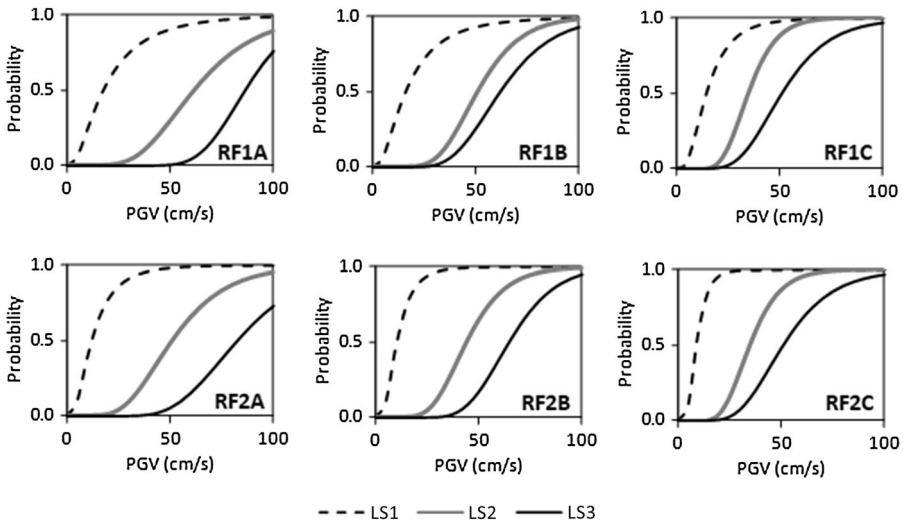
Fig. 8 Fragility curves for RF subclasses using the first group of records categorized based on PGV where the dashed lines correspond to LS_1, the gray solid lines to LS_2, and the black solid lines to LS_3
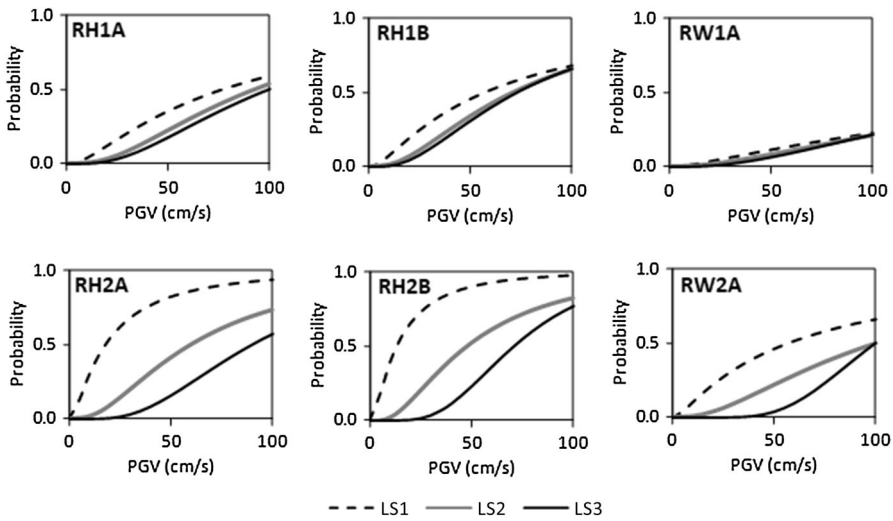

Fig. 9 Fragility curves for RH and RW subclasses using the first group of records categorized based on PGV where the dashed lines correspond to LS_1, the gray solid lines to LS_2, and the black solid lines to LS_3

buildings are significantly affected from the number of stories, structural details, or features regarding earthquake behavior. This is due to the fact that all the lateral resistance comes from the frame system without any additional mechanism. A typical mid-rise RC frame building in Erzincan city that was observed during the field survey is demonstrated in Fig. 11b.

The dual RC buildings with frames and walls (i.e. RH subclasses) also seem to show good seismic performance. Low-rise types are eventually more rigid where the behavior of
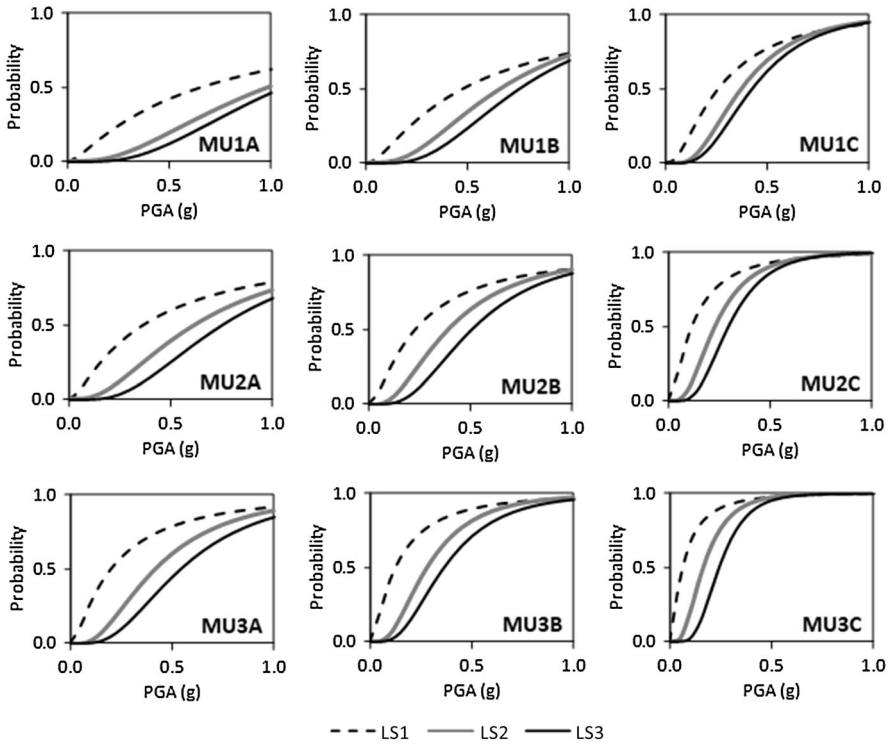
Fig. 10 Fragility curves for masonry subclasses using the second group of records categorized based on PGA where the dashed lines correspond to LS$_1$, the gray solid lines to LS$_2$, and the black solid lines to LS$_3$

Fig. 11 Examples of RC buildings from Erzincan; **a** shear wall RC building (RW), **b** frame RC building (RF), **c** dual RC building (RH)

shear wall dominates; therefore, the fragility curves for RH1A and RH1B are similar to the ones that belong to RW subclasses. In mid-rise types, the effect of frame behavior seems to be much more pronounced where the fragility curves get apart from each other, an indication of relatively a more ductile behavior with a limited range of inelastic response. This type of RC buildings had been built after the 1992 earthquake in Erzincan city (Fig. 11c). Dual RC buildings are known to exhibit adequate behavior in previous major earthquakes in Turkey, which is also reflected in the corresponding fragility curves.

Masonry subclasses seem to exhibit a wide range of seismic response just like the RC frame buildings since they are generally non-engineered structures without any standards

regarding the material quality and the construction technique. Figure 12 shows two masonry buildings from Erzincan city with varying material and construction quality. The best seismic performance is observed for single-story masonry buildings with high level of compliance with the seismic regulations (i.e., MU1A subclass), whereas the worst seismic performance belongs to three-story masonry buildings with low level of compliance with the seismic regulations (i.e., MU3C subclass). For all MU subclasses, the fragility curves are close to each other, indicating that the ductility capacities of these structures are limited (Fig. 10). According to the field observations after major earthquakes in Turkey, when masonry buildings sustain some damage during the earthquake, the propagation of damage is very rapid, causing brittle failure of the structures without showing any adequate capacity for inelastic action.

Above observations show that the fragility curve sets of building subclasses can simulate the inherent characteristics of the buildings in the study region in justifiable terms. Then, the use of this fragility information for seismic damage estimation in Erzincan is validated.

6 Simulation-based seismic damage estimation in Erzincan

In this section, first the methodology for seismic damage estimation is presented followed by a verification exercise, where the estimated damage for the 1992 Erzincan earthquake is compared against the observed one. Next, the potential seismic damage for a scenario event of Mw = 7.0 is presented as a prediction exercise.

6.1 Methodology

Most of the existing damage estimates in the literature are in the form of disaggregated numbers, which makes direct evaluation of damage difficult (Lang et al. 2008; Bal et al. 2010). However, damage estimates in terms of total economic loss, casualty estimates, or mean damage ratio are the most appropriate parameters representing damage levels. Assessment of total economic loss as well as casualty estimates involves reliable replacement cost data and information related to the structural damage as well as the number of occupants present in the building at the time of the earthquake, respectively. Therefore, in the present study, mean damage ratio (MDR) that expresses the

Fig. 12 Examples of masonry buildings from Erzincan with varying material and construction quality

disaggregated damage estimates with a single value as implemented by Askan and Yucemen (2010) is chosen. For the computation of MDR, damage probability matrix (DPM), as introduced by Whitman et al. (1997), is employed. Each column of DPM expresses a constant level of ground motion intensity, while each row of this matrix stands for a certain damage state. Therefore, each element of this matrix, denoted as $P(DS, I)$, indicates the probability of experiencing a certain damage state (DS) when the structure under consideration is subjected to a specified ground motion with intensity level of I:

$$P_k(DS, I) \ = \ \frac{N(DS, I)}{N(I)}, \tag{3}$$

where $N(I)$ is the number of kth-type of buildings in the area subjected to a ground motion of intensity I and $N(DS, I)$ is the number of structures in damage state (DS), among the $N(I)$ buildings.

The general form of a DPM proposed for Turkey by Gürpinar et al. (1978) is given in Table 5. The values in this table reveal that the damage states are separated into five different groups as no damage (N), light damage (L), moderate damage (M), heavy damage (H), and collapse (C). Each damage state corresponds to the degree of structural or non-structural damage for each building type and for each intensity level. Damage ratio (DR) is defined as the ratio of the cost of repairing the earthquake damage to the replacement cost of the building. This parameter takes values in between 0 and 100% and may differ even for the same building type under the similar seismic excitation, due to several factors including variation in soil properties, material conditions, and duration of ground shaking. Therefore, for the sake of simplicity in the process of calculation of MDR from DPM, a single quantitative value named as central damage ratio (CDR) for each damage state is assigned. The range of damage index and the central damage ratios corresponding to the mentioned five damage states proposed by this study are listed in Table 5.

It must be noted that a DPM can be constructed empirically with damage data in the field or computed from theoretical models such as the method proposed herein. There is a close relationship in between fragility curves and DPMs such that the information provided by a fragility curve can be converted to build a DPM. Figure 13 presents the procedure for conversion of a fragility curve to a DPM. The damage information corresponding to each column of the DPM is obtained by intersecting the fragility curve set with vertical lines (dashed lines in Fig. 13) at particular intensity levels. Then, to determine the damage state probabilities, the portions between any two limit states in these vertical alignments are calculated. For the present study, intensity level (IL) takes values corresponding to the intensity parameters of PGV and PGA, which are estimated at each district center for each

Table 5 General form of damage probability matrix given by Gürpinar et al. (1978)

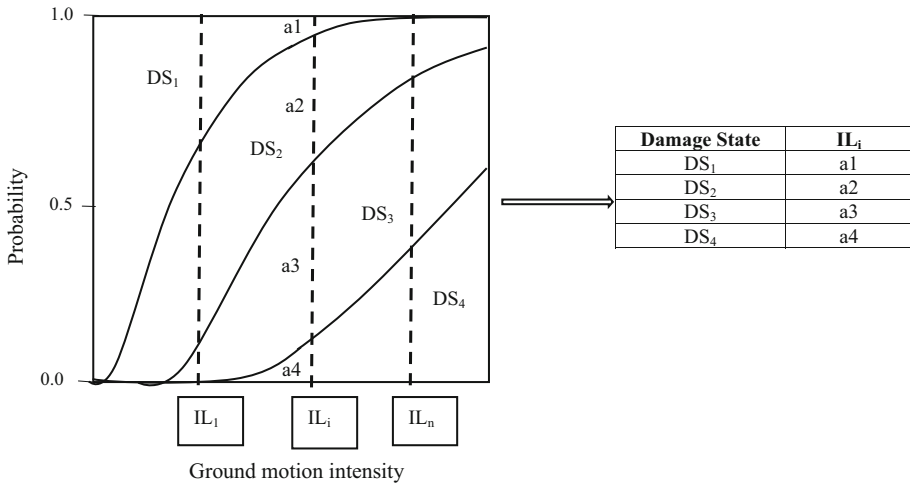| Damage state (DS)	Damage ratio (DR %)	Central damage ratio (CDR %)	Ground motion intensity parameter, I (MMI, PGA, PGV, etc.)
None	0–1	0	Damage state probabilities, $P(DS, I)$
Light	1–10	5	
Moderate	10–50	30	
Heavy	50–90	70	
Collapse	90–100	100	

Fig. 13 Conversion from a set of fragility curves to DPM

scenario event. In this study, since a certain fragility curve set corresponding to a specified building class is derived for three limit states, the constructed DPM has four damage states as none (DS1), light (DS2), moderate (DS3), and severe (DS4). It is noted that both heavy and collapse damage states of Table 5 are considered as a single damage state (severe) with CDR of 85%. For the other damage states, the statistical values of CDRs are taken from Table 5.

To express the damage ratios in a more compact and comparable manner, the discrete values corresponding to each intensity level are converted to a single value as MDR. MDR is expressed as follows:

$$\text{MDR}(I) = \sum_{\text{DS}} P_k(\text{DS}, I) \cdot \text{CDR}(\text{DS}), \tag{4}$$

where CDR(DS) represents the central damage ratio corresponding to damage state DS.

6.2 Applications in the study region

To evaluate the efficiency of the proposed methodology in predicting actual damage distribution of the study area, the proposed method is first applied for the 1992 Erzincan earthquake. Then, as a sample for the prediction of potential losses, the seismic damage for scenario event of Mw = 7.0 is calculated. For this purpose, a total of 16 residential districts in Erzincan city with available building data are selected. The steps for damage assessment are summarized as follows:

- For the simulation of the 1992 Erzincan earthquake (Mw = 6.6) and scenario event with Mw = 7.0, synthetic records for the selected residential areas are collected.
- Since fragility curves of RC and masonry buildings are derived in terms of PGV and PGA, respectively, PGA and PGV values corresponding to center of each considered district are obtained from the synthetic records.
- For the selected districts, percent distribution of the buildings with respect to the structural type as well as number of stories is attained.

- Using the derived fragility curves, DPMs for all building types in each district under the given ground motion value are developed.
- Finally, through percent distribution of buildings in the selected locations, a single MDR is calculated for each residential area.

The estimated ground motion amplitudes in terms of both PGA and PGV for the 1992 Erzincan scenario earthquake (Mw = 6.6) and scenario event with Mw = 7.0 are listed in Table 6. Table 7 represents percent distribution of the buildings with respect to structural system and number of stories in the selected residential areas compiled from the walk-down survey. The observed MDR values for the 1992 Erzincan earthquake are adopted from Sucuoğlu and Tokay (1992), Şengezer (1993), and Erdik et al. (1994). Figure 14(a) presents distribution of the observed MDRs for the selected residential districts, where N/A data correspond to the residential districts in which observed damage levels during the 1992 Erzincan earthquake are not available.

Finally, distribution of the estimated MDRs for the selected residential districts is illustrated in Fig. 14b, where N/A data correspond to the residential districts in which the building information is not available. Comparison of the observed and estimated damage levels for the 1992 Erzincan earthquake demonstrates that for almost 75% of the residential areas, the results are in close agreement. For the other locations, the estimated damage levels are found to be larger than the observed ones. These differences may be attributed to the subjectivity in assigning damage states for the buildings in the field. After validating the method for the 1992 earthquake, the anticipated potential seismic damage for the scenario event of Mw = 7.0 is also computed and presented in Fig. 15. The damage

Table 6 Estimated PGA and PGV for the 1992 Erzincan scenario earthquake and scenario event with Mw = 7.0

District	Node no.	Latitude	Longitude	The 1992 Erzincan scenario earthquake (Mw = 6.6)		Scenario event with Mw = 7.0	
				PGA (g)	PGV (cm/s)	PGA (g)	PGV (cm/s)
İnönü	91	39.7505	39.4857	0.48	22.12	1.06	65.84
İzzetpaşa	92	39.7401	39.5083	0.65	53.51	0.82	59.43
Akşemsettin	94	39.7506	39.5148	0.64	72.19	1.05	55.42
Arslanlı	95	39.7595	39.483	0.45	25.50	1.03	39.62
Atatürk	96	39.7492	39.4955	0.39	23.79	0.98	58.37
Bahçelievler	97	39.7512	39.4757	0.44	50.34	1.06	61.55
Barbaros	99	39.7542	39.5037	0.71	40.37	0.90	62.99
Cumhuriyet	100	39.7594	39.4967	0.74	55.97	0.84	42.84
Ergenekon	101	39.7516	39.4641	0.35	23.06	0.96	102.91
Halitpaşa	104	39.744	39.4789	0.37	29.13	0.85	50.78
Hocabey	105	39.7416	39.4849	0.42	29.27	0.68	42.33
Kızılay	108	39.7448	39.4897	0.64	37.29	0.84	52.91
Mimar Sinan	109	39.743	39.4662	0.65	62.97	0.86	53.53
Yavuz Selim	112	39.7581	39.4738	0.56	61.75	0.94	101.70
Yeni Mahalle	113	39.7574	39.4901	0.40	30.39	0.87	38.34
Fatih	102	39.7461	39.511	0.70	50.94	1.21	95.10

Table 7 Percent distribution of the buildings with respect to structural system as well as number of stories in the Erzincan region

| District	Node no.	Latitude	Longitude	RC (%)	MU (%)	Low-rise RC (%)	Mid-rise RC (%)	One-story MU (%)	Two-story MU (%)	Three-story MU (%)
İnönü	91	39.7505	39.4857	43	57	90	10	40	44	16
İzzetpaşa	92	39.7401	39.5083	16	84	99	1	84	14	2
Akşemsettin	94	39.7506	39.5148	10	90	92	8	90	8	2
Arslanlı	95	39.7595	39.483	50	50	81	19	45	25	30
Atatürk	96	39.7492	39.4955	40	60	86	14	25	39	36
Bahçelievler	97	39.7512	39.4757	49	51	90	14	24	35	41
Barbaros	99	39.7542	39.5037	20	80	100	0	41	34	25
Cumhuriyet	100	39.7594	39.4967	15	85	90	10	40	44	16
Ergenekon	101	39.7516	39.4641	89	11	16	84	40	34	26
Halitpaşa	104	39.744	39.4789	6	94	97	3	65	25	10
Hocabey	105	39.7416	39.4849	4	96	99	1	74	19	7
Kızılay	108	39.7448	39.4897	10	90	99	1	95	2	3
Mimar Sinan	109	39.743	39.4662	78	22	84	16	48	35	17
Yavuz Selim	112	39.7581	39.4738	70	30	69	31	23	34	43
Yeni	113	39.7574	39.4901	27	73	91	9	59	26	15
Fatih	102	39.7461	39.511	16	84	88	12	86	7	7
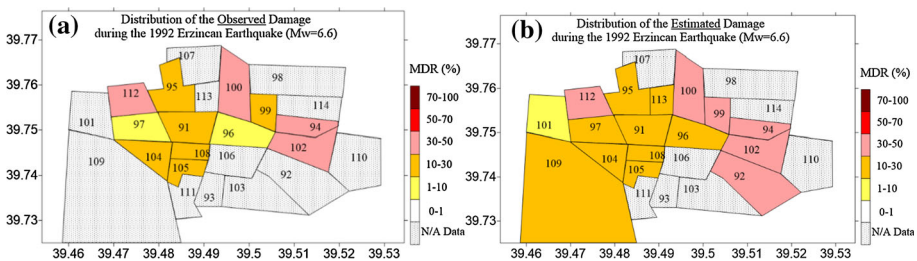
Fig. 14 Distribution of the **a** observed, **b** estimated MDRs in the Erzincan region for the 1992 Erzincan earthquake

estimates for the scenario event of Mw = 7.0 reveal that six of the residential areas experience severe damage (50% <= MDR <=100%). However, the estimated damage in the rest of the residential areas is moderate (10% <= MDR <=50%). Therefore, for scenario event of Mw = 7.0, the estimated damage levels show that the Erzincan city center is subjected to the moderate to heavy damage levels in the selected residential areas, which is consistent with the regional seismicity and the structural vulnerability.
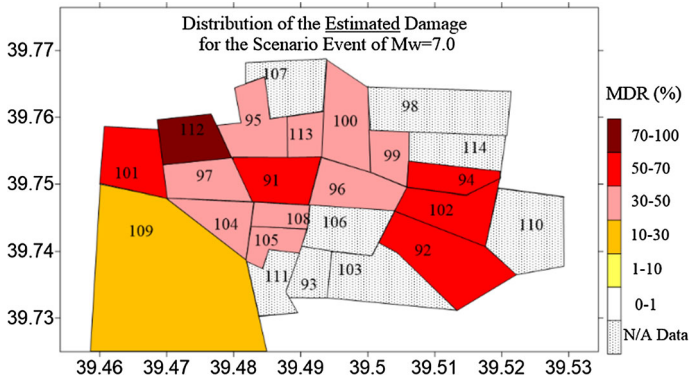
Fig. 15 Distribution of the estimated MDRs in the Erzincan region for scenario event of Mw = 7.0

7 Conclusions

In this study, seismic damage estimation of Erzincan is performed considering both regional seismic hazard and local building data. For this purpose, stochastic finite-fault methodology is applied to generate simulated time histories compatible with regional seismicity. The use of simulations provides a large set of records that include the inherent variability in terms of source, path, and site effects. Then, a comprehensive building database corresponding to the study area is assembled from a field survey. Structural damage is estimated for all residential districts in the study area for the 1992 earthquake and a scenario event with Mw = 7.0.

Similar to the other seismic loss assessment methodologies, the methodology presented herein contains inherent uncertainties arising from various sources such as modeling errors involved with the ground motion simulation technique, assumption of input parameters, building data, fragility, and damage estimation methodology. In spite of these uncertainties, based on the results of this study, a reasonable match between the observations and computed results for the 1992 Erzincan earthquake is obtained. It is observed that locally derived fragility curves involving both regional seismic properties considering the specific characteristics of the earthquake rupture and local building models yield damage rates that match closely with observations. Validations against the observed damage levels show that the simulated ground motions used as input to local ESDOF building models can effectively estimate the spatial distribution of damages from large events in urban areas. This result indicates that the existing uncertainties do not yield significant errors in the estimations.

Besides, the estimated damage levels for a scenario event of Mw = 7.0 in the city center reveal that Erzincan is under significant seismic threat due to its close distance from the fault system in the North, soft soil conditions within Erzincan basin as well as the seismic vulnerability of the building stock in the respective area. Thus, to mitigate potential future earthquake losses in the region, the built environment must be evaluated for seismic safety in detail.

Results of this study revealed the significance of using local seismotectonic and structural properties in damage estimation process. It is recommended that future studies use similar approaches for accurate damage and loss estimations.

References

Akinci A, Malagnini L, Herrmann RB, Pino NA, Scognamiglio L, Eyidogan H (2001) High-frequency ground motion in the Erzincan region, Turkey: inferences from small earthquakes. Bull Seismol Soc Am 91(6):1446–1455. https://doi.org/10.1785/0120010125

Akkar S, Sucuoğlu H, Yakut A (2005) Displacement-based fragility functions for low and mid-rise ordinary concrete buildings. Earthq Spectra 21(4):901–927. https://doi.org/10.1193/1.2084232

Akyuz HS, Hartleb R, Barka A, Altunel E, Sunal G, Meyer B, Armijo R (2002) Surface rupture and slip distribution of the 12 November 1999 Düzce earthquake (M 7.1), North Anatolian fault, Bolu, Turkey. Bull Seismol Soc Am 92(1):61–66. https://doi.org/10.1785/0120000840

Anderson JG, Hough SE (1984) A model for the shape of the Fourier amplitude spectrum of acceleration at high frequencies. Bull Seismol Soc Am 74(5):1969–1993

Askan A, Yucemen MS (2010) Probabilistic methods for the estimation of potential seismic damage: application to reinforced concrete buildings in Turkey. Struct Saf 32(4):262–271. https://doi.org/10.1016/j.strusafe.2010.04.001

Askan A, Sisman FN, Ugurhan B (2013) Stochastic strong ground motion simulations in sparsely monitored regions: a validation and sensitivity study on the 13 March 1992 Erzincan (Turkey) earthquake. Soil Dyn Earthq Eng 55:170–181. https://doi.org/10.1016/j.soildyn.2013.09.014

Askan A, Asten M, Erberik MA, Erkmen C, Karimzadeh S, Kilic N, Sisman FN, Yakut A (2015a) Seismic damage assessment of Erzincan, Turkish national union of geodesy and geophysics project. Project no: TUJJB-UDP-01-12, Ankara

Askan A, Karimzadeh S, Asten M, Kiliç N, Sisman FN, Erkmen C (2015b) Assessment of seismic hazard in the Erzincan (Turkey) region: construction of local velocity models and evaluation of potential ground motions. Turk J Earth Sci 24(6):529–565. https://doi.org/10.3906/yer-1503-8

ATC (1996) Seismic evaluation and retrofit of concrete buildings. ATC-40, Applied Technology Council, Redwood City, 1

Bal IE, Bommer JJ, Stafford PJ, Crowley H, Pinho R (2010) The influence of geographical resolution of urban exposure data in an earthquake loss model for Istanbul. Earthq Spectra 26(3):619–634. https://doi.org/10.1193/1.3459127

Beresnev I, Atkinson GM (1964) Modeling finite-fault radiation from the ω^n spectrum. Bull Seismol Soc Am 87(1):67–84

Biggs JM (1964) Introduction to structural dynamics. McGraw Hill Company, New York, p 3

Boore DM (1983) Stochastic simulation of high-frequency ground motions based on seismological models of the radiated spectra. Bull Seismol Soc Am 73(6A):1865–1894

BSSC (1997) NEHRP guidelines for the seismic rehabilitation of buildings. FEMA-273, developed by ATC for FEMA, Washington, DC

Clough R, Johnston SB (1966) Effect of stiffness degradation on earthquake ductility requirements. In: Proceedings, 2nd Japan national conference on earthquake engineering, pp 227–232

Erberik MA (2008a) Fragility-based assessment of typical mid-rise and low-rise RC buildings in Turkey. Eng Struct 30(5):1360–1374. https://doi.org/10.1016/j.engstruct.2007.07.016

Erberik MA (2008b) Generation of fragility curves for Turkish masonry buildings considering in-plane failure modes. Earthq Eng Struct D 37(3):387–405. https://doi.org/10.1002/eqe.760

Erdik M, Yüzügüllü O, Karakoc Yilmaz C, Akkas N (1994) March 13, 1992 Erzincan (Turkey) earthquake. In: Earthquake engineering 10th world conference

Fajfar P, Fischinger M (1988) N2—a method for non-linear seismic analysis of regular structures. In: Proceedings of the 9th world conference on earthquake engineering, vol 5, pp 111–116

Frankel A (1993) Three-dimensional simulations of the ground motions in the San Bernardino valley, California, for hypothetical earthquakes on the San Andreas Fault. Bull Seismol Soc Am 83(4):1020–1041

Gürpinar A, Abali M, Yücemen MS, Yesilcay Y (1978) Feasibility of obligatory earthquake insurance in Turkey. Earthquake Engineering Research Center, Civil Engineering Department, Middle East Technical University, Ankara 78-05 (**in Turkish**)

Hartzell SH (1978) Earthquake aftershocks as Green's functions. Geophys Res Lett 5(1):1–4. https://doi.org/10.1029/GL005i001p00001

Hsieh MH, Lee BJ, Lei TC, Lin JY (2013) Development of medium-and low-rise reinforced concrete building fragility curves based on Chi–Chi Earthquake data. Nat Hazards 69(1):695–728. https://doi.org/10.1007/s11069-013-0733-8

Ibarra LF, Krawinkler H (2005) Global collapse of frame structures under seismic excitations. Rep. no. TB 152, The John A. Blume Earthquake Engineering Center, Stanford University, Stanford

Ibarra LF, Medina RA, Krawinkler H (2005) Hysteretic models that incorporate strength and stiffness deterioration. Earthq Eng Struct D 34(12):1489–1511. https://doi.org/10.1002/eqe.495

Kamae K, Irikura K, Pitarka A (1998) A technique for simulating strong ground motion using Hybrid Green's function. Bull Seismol Soc Am 88(2):357–367

Kappos AJ, Stylianidis KC, Pitilakis K (1998) Development of seismic risk scenarios based on a hybrid method of vulnerability assessment. Nat Hazards 17(2):177–192. https://doi.org/10.1023/A:1008083021022

Karimzadeh S, Askan A, Erberik MA, Yakut A (2015) Multicomponent seismic loss estimation on the North Anatolian Fault Zone (Turkey). Paper no.: NH13B-1920, American Geophysical Union, San Francisco

Kircil MS, Polat Z (2006) Fragility analysis of R/C frame buildings. Eng Struct 28(9):1335–1345

Lang DH, Molina S, Lindholm CD (2008) Towards near-real-time damage estimation using a CSM-based tool for seismic risk assessment. J Earthq Eng 12(S2):199–210. https://doi.org/10.1080/13632460802014055

Lignos DG, Krawinkler H (2010) Deterioration modeling of steel components in support of collapse prediction of steel moment frames under earthquake loading. J Struct Eng 137(11):1291–1302. https://doi.org/10.1061/(ASCE)ST.1943-541X.0000376

Lignos DG, Krawinkler H (2012) Development and utilization of structural component databases for performance-based earthquake engineering. J Struct Eng 139(8):1382–1394. https://doi.org/10.1061/(ASCE)ST.1943-541X.0000646

Mai PM, Imperatori W, Olsen KB (2010) Hybrid broadband ground-motion simulations: Combining long-period deterministic synthetics with high-frequency multiple S-to-S back-scattering. Bull Seismol Soc Am 100(5A):2124–2142. https://doi.org/10.1785/0120080194

Mohammadioun B, Serva L (2001) Stress drop, slip type, earthquake magnitude, and seismic hazard. Bull Seismol Soc Am 91(4):694–707. https://doi.org/10.1785/0120000067

Motazedian D, Atkinson GM (2005) Stochastic finite-fault modeling based on a dynamic corner frequency. Bull Seismol Soc Am 95(3):995–1010. https://doi.org/10.1785/0120030207

Olsen KB, Archuleta RJ, Matarese JR (1996) Three-dimensional simulation of a magnitude 7.75 earthquake on the San Andreas fault. Science 270(5242):1628

OpenSees 2.4.5, Computer Software, University of California, Berkeley. http://opensees.berkeley.edu. Accessed 12 Dec 2014

Pitarka A, Somerville P, Fukushima Y, Uetake T, Irikura K (2000) Simulation of near-fault strong ground motion using Hybrid Green's functions. Bull Seismol Soc Am 90(3):566–586. https://doi.org/10.1785/0119990108

Qi X, Moehle JP (1991) Displacement design approach for reinforced concrete structures subjected to earthquakes. Earthquake Engineering Research Center, College of Engineering/University of California, 91:(2)

Saiidi M, Sozen MA (1981) Simple nonlinear seismic analysis of R/C structures. J Struct Div 107(5):937–953

Şengezer BS (1993) The damage distribution during March 13, 1992 Erzincan earthquake. In: Proceedings. 2nd national earthquake engineering conference, pp 404–415

Sørensen MB, Lang DH (2014) Incorporating simulated ground motion in seismic risk assessment-application to the lower Indian himalayas. Earthq Spectra 31(1):71–95. https://doi.org/10.1193/010412EQS001M

Sucuoğlu H, Tokyay M (1992) 13 Mart 1992 Erzincan earthquake engineering report. Civil Engineering Department, Ankara, p 102

Tesfamariam S, Goda K (2015) Loss estimation for non-ductile reinforced concrete building in Victoria, British Columbia, Canada: effects of mega-thrust Mw9-class subduction earthquakes and aftershocks. Earthq Eng Struct D 44(13):2303–2320. https://doi.org/10.1002/eqe.2585

TUIK. http://www.tuik.gov.tr/Web2013/iletisim/iletisim.html. Accessed 19 Sept 2013

Ucar T, Duzgun M (2013) Derivation of analytical fragility curves for RC buildings based on nonlinear pushover analysis. IMO Teknik Dergi 24(3):6421–6446 (In Turkish)

Ugurhan B, Askan A (2010) Stochastic strong ground motion simulation of the 12 November 1999 Düzce (Turkey) earthquake using a dynamic corner frequency approach. Bull Seismol Soc Am 100(4):1498–1512. https://doi.org/10.1785/0120090358

Ugurhan B, Askan A, Erberik MA (2011) A methodology for seismic loss estimation in urban regions based on ground-motion simulations. Bull Seismol Soc Am 101(2):710–725. https://doi.org/10.1785/0120100159

Wells DL, Coppersmith KJ (1994) New empirical relationships among magnitude, rupture length, rupture width, rupture area and surface displacement. Bull Seismol Soc Am 84(4):974–1002

Whitman RV, Anagnos T, Kircher CA, Lagorio HJ, Lawson RS, Schneider P (1997) Development of a national earthquake loss estimation methodology. Earthq Spectra 13(4):643–661. https://doi.org/10.1193/1.1585973

Yakut A, Ozcebe G, Yucemen MS (2006) Seismic vulnerability assessment using regional empirical data. Earthq Eng Struct Dyn 35(10):1187–1202. https://doi.org/10.1002/eqe.572

Yong C, Ling C, Güendel F, Kulhánek O, Juan L (2002) Seismic hazard and loss estimation for Central America. Nat Hazards 25(2):161–175. https://doi.org/10.1023/A:1013722926563